QSAR & Combinatorial Science QCS

Use of Quantitative Structure-activity Relationship to Model the Photoinduced Toxicity of Anthracene and Oxygenated Anthracenes

Ali Mallakin[a]*, Paul G. Mezey[b], Zbigniew Zimpel[c], Kenneth S. Berenhaut[d], Bruce M. Greenberg[e] and D. George Dixon[e]

[a] Department of Pathology, Wake Forest University Health Sciences, 2102 Gray Building, Medical Center Blvd., Winston-Salem, NC 27157, USA, Phone: 336-716-3975, Fax: 336-716-6757, E-mail: amallaki@wfubmc.edu.
[b] Department of Chemistry, Department of Physics and Physical Oceanography, Memorial University of Newfoundland, St. John's, NL, A1B 3X7, Canada
[c] Department of Chemistry, 110 Science Place, University of Saskatchewan, Saskatoon, SK S7N 5C9, Canada
[d] Department of Mathematics, Wake Forest University, Winston-Salem, NC 27109, USA
[e] Department of Biology, University of Waterloo, Waterloo, ON N2L 3G1, Canada

Keywords: QSAR, anthracene, photoinduced toxicity, PAHs, UVB

Received: January 6, 2005; Accepted: February 19, 2005

Abstract

Polycyclic aromatic hydrocarbons (PAHs) are known to exhibit photoinduced toxicity to organisms, especially in the presence of ultraviolet irradiation. Oxidation is the most common photochemical reaction of anthracene (ANT) and ANT derivatives. Quinones, hydroxy-quinones, diols, and aldehydes are the resultant products. Different ANT photoproducts have different impact on biological organisms. The structure of these molecules contains information concerning their toxicity. From two main bioenergetic pathways in aerobic organisms (respiration and photosynthesis), we have previously reported the inhibition of photosynthesis by ANT derivatives. We showed that inhibition of photosynthesis is a reliable assay of xenobiotic stress. To study the correlation between chemical structures and toxicity, precise structure of anthracene (ANT), anthraquinone (ATQ) and eleven hydroxyanthraquinones (hATQs) were constructed. A numerical comparison of molecular shape codes was used for shape comparison and similarity analysis. The data sets for growth inhibition showed good correlations to the shape similarity. Both the one ring and whole molecule similarities of ANT, ATQ and hATQs showed a good correlation with the empirical whole organism toxicity data. The IC_{50} values for F_V/F_M and F_Q/F_M were plotted against hyperbolic dependencies of one-ring and whole molecule similarity to determine their predictive capacity. The two data sets for F_Q/F_M and F_V/F_M have reasonable regression coefficients, and both were found to be excellent bioindicators of effects. In this study correlation between the shape of chemicals and the biological activity provides necessary information related to toxicity of hazard chemicals based on chemical and biological properties of their reactions.

1 Introduction

Polycyclic aromatic hydrocarbons (PAHs), a group of toxic and mutagenic contaminants, are both ubiquitous and highly hydrophobic [1, 2]. Photoinduced processes involving these chemicals are observed as increased toxicity of PAHs in the presence of simulated solar radiation [3, 4]. PAHs strongly absorb solar ultraviolet (UV) radiation, resulting in photomodification usually via oxidation reactions [5]. Previous work has shown that photomodification of ANT results in complex mixtures of photoproducts that are more toxic than the parent compound [3]. It was further demonstrated that photomodified PAHs are biologi-

Abbreviations: Concentration that produces an adverse effect in 50% of the exposed organisms: EC_{50}; Concentration that produces a growth inhibition in 50% of the exposed organisms: IC_{50}; Dihydroxyanthraquinone: dhATQ; WMS.: Whole Molecule Similarity; FS: Fragment Similarity; F_M: Maximum Fluorescence; F_V: Variable Fluorescence; GI: Growth Inhibition; mM/l: millimole per liter; MIDCO: Molecular Isodensity Contour; Quantitative structure-activity relationship: QSAR; PAH: Polycyclic aromatic hydrocarbon; PSI: Photosystem I; PSII: Photosystem II; UV: Ultraviolet

 DOI: 10.1002/qsar.200530003

cally damaging to the photosynthetic apparatus [6]. Different ANT photoproducts have distinctly different toxicities. Consequently, the structures of molecules should contain information concerning their toxicological risks. The molecular charge density cloud contains all molecular information in a very special form, governed by complicated laws of quantum chemistry, but fortunately, the manifestations of this information can be studied using correlations between electron density shape features and experimentally determined properties. The concept that molecular electron densities contain all informations about the molecule has been proven in 1964, in the work that won a Nobel Prize for W. Kohn in 1998 [7]. Later it was proven that, any small positive volume of the electron density cloud already contains the complete information, giving justification for local shape analysis of molecular electron density clouds [8].

The same molecule, under the same conditions, is expected to generate the same toxicological response, and highly similar molecules are expected to generate a similar toxicological response [8]. One may regard the similarity-based molecular electron density-toxicological effect correlation method as analogous to an actual toxicological black box experiment: input the molecule into the black box, out comes the toxicological effect. How many and what intermediate steps and stages are within the black box are poorly understood, yet the following is still valid: highly similar input molecules are likely to produce similar toxicological results, whether or not one knows what actual conformations, metabolites, and decomposition products are produced. Study of toxicity starts with the molecule, and ends with the measured toxic effect, however complex the black box is, so we have rather complete molecular information. These are the reasons for the success and justification of the QSAR approach. This approach lies at the basis of the present study, in which molecular shape analysis was used to compare the electron densities of the molecules to their toxicities.

Our understanding of toxicology can benefit from molecular shape analysis [9–13]. Molecular shape and numerical evaluation of molecular similarity can be used in quantitative structure activity relationships (QSARs) [14–16]. The nuclear distribution and electron density cloud of a molecule should be able to describe its biological and chemical reactivity. The relationships between these parameters and molecular hardness [17, 18] shown previously explain variation of this endpoint for much larger set of PAHs and other aromatic chemicals [19, 20]. However, because the electron densities of organic molecules also describe their nuclear distribution, in most instances it alone can describe the reactivity of a molecule. The electron density clouds of organic compounds represent fuzzy molecular bodies that provide a mode for analyzing shapes of the molecules [21–24]. If two molecules react differently, these differences should be reflected in their electron density clouds. Theoretically, for the reaction of organic molecules in biologically relevant settings, no other quantum considerations of the molecule is required [16, 20].

Accurate electron density shape representations of molecules were developed to better describe the toxicity of different molecules [15, 16]. This methodology allows the incorporation of π-orbitals into the electron cloud surfaces. This is a key element in understanding the correlation between toxic properties and/or biochemical reactivities of molecules, and specific shape features of their electron density clouds. Current techniques using a computational microscope method of quantum chemical and *ab initio* molecular descriptions, based on fuzzy density fragments, allow one to generate high-resolution electron density maps of PAHs [15]. Previous study has used these computer generated molecules to develop a QSAR model describing the photoinduced toxicity of intact PAHs [16]. It was shown that the computer programs have the capability of recognizing and evaluating similarities within a selected molecular family (e.g. PAHs), and correlating local and global shape features with primary toxicological data. This led to the finding that global shape and single ring shape could be associated with the photosensitization and photomodification activities of intact PAHs, respectively.

To extend the above QSAR work, a suite of anthracene photoproducts (ATQ and hATQs) were selected for the development of a shape fragment database for QSAR modelling. Previously we evaluated the toxicity of different ANT photoproducts under actinic radiation [3]. Also it was shown that toxicity was due in large part to inhibition of photosynthesis [6]. We reported the effects of oxygenated ANTs on photosynthesis *in vivo*, and we determined the IC_{50}s for F_V/F_M (PSII activity) and F_Q/F_M (activity downstream from PSII) [6]. The data obtained by monitoring the induction kinetics of endogenous chlorophyll α (Chl α) fluorescence [6]. In this study, a complete description of the electron shape-density cloud of each molecule was generated at both high and low electron density ranges. Computer modelling was used to relate the shape density clouds for each molecule to the toxicological data published previously [3, 6]. Further, it was important to determine if the same shape model that describes toxicity at the whole organism level would predict toxicity at the level of photosynthesis.

2 Methods

2.1 Chemicals

Anthracene (ANT), anthraquinone (ATQ), and eleven hydroxyanthraquinone (hATQ): 1-hydroxyATQ (1-hATQ), 2-hydroxyATQ (2-hATQ), 1,2-dihydroxyATQ (1,2-dhATQ; alizarin), 1,3-dihydroxyATQ (1,3-dhATQ), 1,4-dihydroxyATQ (1,4-dhATQ; quinizarin), 1,5-dihydroxyATQ (1,5-dhATQ; anthrarufin), 1,8-dihydroxyATQ (1,8-dhATQ), 2,6-dihydroxyATQ (2,6-dhATQ; anthraflavic acid), 1,2,4-

Table 1. Toxicity data used for modelling. Toxicity is inhibition of growth of *L. gibba* by ANT and its photoproducts, and represented as normalized inhibition of growth relative to the control plants. Chemicals tested were at concentrations of 3 mM/l and 12 mM/l based on amount of the parent compounds. EC_{50} values were calculated from full dose response curves and are given in mM/l. Data for 3 mM/l and 12 mM/l inhibition are relative impairment of fluorescence [F_V/F_M control – F_V/F_M treated] / F_V/F_M control, and [F_Q/F_M control - F_Q/F_M treated] / F_Q/F_M control). IC_{50} values for diminishment of F_V/F_M and F_Q/F_M were obtained from full dose response curves (Mallakin *et al*., 2002).

Name of PAH Molecule	Growth Inhibition 3 mM/l	Growth Inhibition 12 mM/l	Growth Inhibition EC_{50}	(F_V/F_M)			(F_Q/F_M) IC_{50} Inhibition		
				IC_{50}	Inhibition		IC_{50}	Inhibition	
					3 mM/l	12		3 mM/l	12
ANT	0.45	0.96	0.8	1.8	0.48	0.46	0.09	0.74	0.92
ATQ	0.43	0.97	0.5	1.6	0.05	0.49	0.03	0.76	1.00
1-hATQ	0.34	0.50	2.4	3.4	0.11	0.09	0.06	0.75	1.00
2-hATQ	1.00	0.99	0.05	0.4	0.62	0.57	0.02	0.81	1.00
1,2-dhATQ	0.22	0.40	2.8	1.7	0.54	0.46	0.6	0.65	0.68
1,3-dhATQ	0.26	0.45	2.5	3.5	0.21	0.18	0.15	0.05	0.8
1,4-dhATQ	0.07	0.22	6.5	20.0	0.20	0.17	20.0	0.08	0.04
1,5-dhATQ	0.05	0.16	15	13.0	0.25	0.22	13.0	0.09	0.2
1,8-dhATQ	0.22	0.41	2.5	16.0	0.32	0.26	8.0	0.37	0.4
2,6-dhATQ	0.02	0.08	12	15.0	0.04	0.06	7.0	0.27	0.36
1,2,4-thATQ	0.07	0.25	6	7.0	0.09	0.13	0.55	0.42	0.6
1,2,5,8-thATQ	0.11	0.17	9.5	10.0	0.12	0.21	1.00	0.45	0.52
1,2,10-thANT	0.05	0.20	10	5.0	0.14	0.36	1.00	0.49	0.56

trihydroxyATQ (1,2,4-thATQ; purpurin), 1,2,5,8-tetrahydroxyATQ (1,2,5,8-thATQ; quinalizarin), 1,2,10-trihydroxy- ANT (1,2,10-thANT; anthrarobin) were the molecules used in this study. Data on their relative experimental toxicity to *L. gibba* [3], and the relevant numerical results of the photosynthetic analysis [6] are listed in Table 1. The toxicity data used for modelling were growth inhibition at 3 mM/l and 12 mM/l. The EC_{50} values for growth inhibition were also used for toxicity modelling. For photosynthesis, diminishment of F_Q/F_M, F_V/F_M and their IC_{50} values at 3 mM/l and 12 mM/l were used respectively. The concentration of test chemicals or chemical mixtures are reported in molar units.

2.2 Molecular shape modelling

The molecular shapes were generated using P. G. Mezey's protocols and computer codes [15, 16]. To begin the process of generating shape maps, precise structures of ANT, ATQ and eleven hATQs were constructed using GAUSSIAN 92 and GSHAPE 90. The Gaussian 92 program package was running on an Alpha DEC 3000 Unix computer. The electron densities for each molecule studied were computed using high-resolution shape fragment databases [16]. The molecular shapes were generated using the shape-group method, in which the molecular shapes were constructed using the molecular isodensity contour (MIDCO) surfaces of calculated quantum mechanical descriptions of the molecules [16]. MIDCO maps used to generate the (a, b)-maps (concise numerical shape representations) were then calculated for each molecule. To test the MIDCOs, visual representations of the molecules were generated (Figure 1). In the MIDCOs, the hydroxy and oxygen groups of the compounds are clearly distinguishable especially at the higher electron densities (Figure 1). The minimum ground-state energy of each molecule was calculated using the closed-shell Hartree-Fock approximation.

To determine the molecular shapes, the internuclear distances of ANT, ATQ and eleven hATQs were optimized using the 6-31G** atomic orbital basis set. The electron density for each molecule and each molecular fragment was entered into a database described in previous papers [15, 16]. The input for the GAUSSIAN calculations were obtained from PDB (photoshop deluxe boundary) files generated using Hyperchem software on an IBM PC computer. Using the shape-group method, (a, b)-maps (electron density shape maps) were computed for each molecule [16]. The shape representation for each chemical was computed in the period of a few days. Such (a, b)-maps are universal discrete representations of the molecular shapes, molecular fragments and whole molecules. In this study, the densities used were 0.1 to 0.001 atomic units (a.u.), where one a.u. corresponds to the electron charge per cubic bohr. These data were analyzed in search of the correlation between shape and toxicity of chemicals, as well as the correlation for inhibition of photosynthetic activity. The goal was to find a correlation between the (a, b)-maps of ANT and the ANT photoproducts and the experimental toxicities. Based on the knowledge of the photoinduced

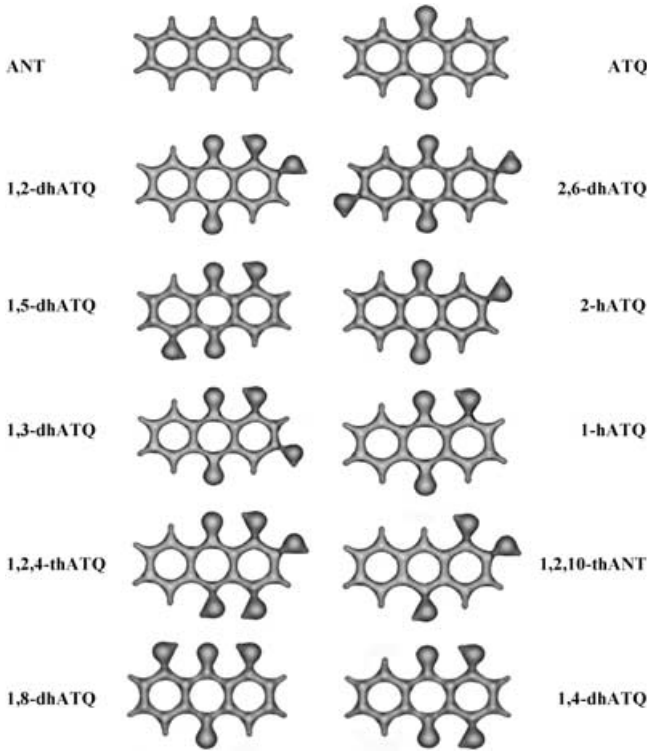

Figure 1. The 0.1 au electron density contours of ANT, ATQ and hATQs. Densities were calculated from MIDCOs of each molecule. The contours shown here are representative of these data.

toxicity of PAHs, one-ring and whole-molecule similarities were generated from the (a, b)-maps [16]. This was shown previously to be a predictor of toxicity for intact PAHs.

The quality of the above computational analysis was determined from the quantum mechanical computations which resulted in the electron densities. The (a, b)-maps were tested for accuracy using the AVS software package on a UNIX computer. This was done at the *ab initio* level using a set of atomic orbital basis functions (expansion functions). Qualities of the shape analysis and shape code computations were also determined by the computed electron densities, which were used to generate graphical displays of the molecules [16].

2.3 Statistical and correlation analysis

Linear regressions were fit to test for correlations between molecular shape and toxicity using the MGLH module of SYSTAT (Version 8.0 for Windows, Systat, Evanston, IL, USA). The quality of fit of the regressions (r^2) and the significance of the regressions (p) were determined with SYSTAT. A four-fold cross validation is used to confirm the significance of the derived models. The shape data also fit hyperbolic functions based on the toxicity data yielding theoretical toxicities, $Y_{theor} = C_0/(1\text{-}C_1X_1)$. Where X_1 is the one-ring or whole molecule similarities, and C_0 and C_1 are the regression coefficients. These hyperbolic fits were then plotted against empirical toxicity and tested for correlations.

3 Results and Discussion

3.1 Whole molecule and central ring similarity

A regression equation was used to estimate the activities of chemicals based on the analysis of their molecular shapes [16, 21, 22]. The (a, b)-maps of ANT, ATQ and eleven hATQs and their fragments were computed to compare their molecular shapes with empirical toxicity data. The quantum chemical accuracy was demonstrated by the *ab initio* quality of the computed electron densities [21]. The accuracy of the application of the shape method was limited to the 6-31G** basis set since the density fragment database has been constructed at this *ab initio* level [21]. A similarity comparison of the shapes of a series of ANT derivatives provided information to better understand the complex nature and hazards of these aromatic compounds. A numerical comparison of molecular shape codes was used for shape comparison and similarity analysis [18, 21]. The similarity of the shape of three-dimensional molecular bodies was quantified and measured by comparing their numerical shape codes (Table 2). To consider the similarity comparison of the shapes of the molecules, the electron distributions were superimposed. The standard methods of comparing matrices was applied to the (a, b)-maps to obtain a numerical measure for their molecular similarity [16]. This comparison did not involve a

Table 2. Results of the numerical shape-analysis and similarities of (a, b)-maps. Whole molecule and fragment similarity for ANT, ATQ and hATQs were analysed. The (a, b)-maps of the whole molecules and their middle rings were compared to the (a, b)-map of 2-hATQ. The degree of similarity with 2-hATQ as a reference structure shown for each molecule.

Compounds	Whole Molecule Similarity *ED 3-1	Fragment Similarity * ED 3-1
ANT	0.63	0.30
ATQ	0.64	0.81
1-hATQ	0.81	0.73
2-hATQ	1.00	1.00
1,2-dhATQ	0.66	0.71
1,3-dhATQ	0.74	0.75
1,4-dhATQ	0.66	0.71
1,5-dhATQ	0.66	0.69
1,8-dhATQ	0.71	0.71
2,6-dhATQ	0.69	0.63
1,2,4-thATQ	0.65	0.72
1,2,5,8-thATQ	0.57	0.66
1,2,10-thANT	0.62	0.47

* **ED 3-1** (**E**lectron **D**ensity $10^{-3} - 10^{-1}$) represents the electron density distribution calculated using *ab initio* Hartree-Fock method at the range of 0.001 to 0.1 au.

visual inspection, rather, an algorithmic shape-similarity evaluation was carried out by computer. This was repeated for all possible pairs of fragments in the molecules (Table 2).

The whole molecule and the middle ring fragment of 2-hATQ, the most toxic molecule among the selected chemicals, were compared to the most similar fragments of other compounds. Thus, the (a, b)-maps of 2-hATQ and its fragments were compared to (a, b)-maps of other molecules and their fragments. The whole molecule and central ring similarities are presented in Table 2.

When the whole molecule similarity was examined, the range of similarity was as low as 0.57 for 1,2,5,8-thATQ relative to 2-hATQ (1.0). Surprisingly, ANT (0.63) and 1,2,10-thANT (0.62) were more similar to 2-hATQ than 1,2,5,8-thATQ, even though they did not have a central quinone ring. At the whole molecule level, 1,2-dhATQ (0.66) was also less similar to 2-hATQ than either 1,3-dhATQ (0.74) and 1,8-dhATQ (0.71), even though neither of the latter molecules had a hydroxy at the second position. Interestingly, three of the five dhATQs had identical whole similarities to 2-hATQ. Eleven of the thirteen values for whole molecular similarities are between 0.74 and 0.57 with nine of them between 0.71 and 0.62, and with seven of these between 0.66 and 0.62 (Table 2).

The numerical values of fragment similarities based on the central quinone ring were spread over a larger range; from 0.30 for ANT to 1.0 for 2-hATQ. As would be expected, the two nonquinone molecules (ANT and 1,2,10-thANT) had the least similarity with the reference molecule (2-hATQ). The most similar molecule to 2-hATQ by this measure was ATQ, not one of the hATQs. Once again three of the five dhATQs had identical similarities relative to 2-hATQ, but these were not the same three molecules that had identical similarities to 2-hATQ at the whole molecule level (Table 2). The similarities of (a, b)-maps were then correlated with experimental toxicities. Correlations were performed in two steps. First the correlations of the (a, b)-maps for the central ring were examined, with respect to the middle ring of 2-hATQ molecule as reference. Second, the similarities of the (a, b)-maps of the whole molecules were analysed and compared with 2-hATQ molecule. The similarity measures were then correlated with toxic activities, forming the basis of QSAR models.

3.2 Correlation between shape analysis and toxicity data

The similarities of the (a, b)-maps of single fragments, with respect to the middle ring of 2-hATQ as a reference, were first examined. 2-hATQ was used as the reference point because it is the most toxic of the chemicals tested. The fragment similarities were compared to the toxicity data from our previous study (Table 1), [3]. Growth inhibition for all 13 chemicals in this study was plotted against the fragment similarities (Figure 2). A very weak correlation between the middle ring similarities and toxicity data

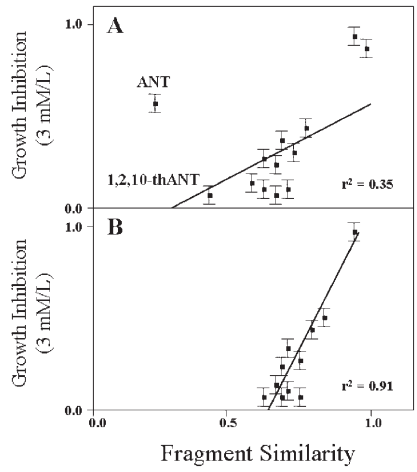

Figure 2. A) Correlation between growth inhibition (3 mM/l) and fragment similarity with all 13 chemicals including ANT and 1,2,10-thANT. B) Correlation between growth inhibition (3 mM/l) and fragment similarity without ANT and 1,2,10-thANT. The electron density range used was 10^{-3} to 10^{-1} au.

was observed. However, one can see that ANT and 1,2,10-thANT may be outliers. Thus, these two compounds were excluded in an attempt to present a better linear fit for the rest of hATQs examined. The elimination of ANT and 1,2,10-thANT was motivated by their structural differences (they are the only non-quinone molecules) and they had the lowest similarity to 2-hATQ for the single fragment data (Table 2). In addition they both can be photomodified rapidly to quinones [5]. So most of their toxic activity is probably due to the generated quinones. When ANT and 1,2,10-thANT excluded from the graph the regression was improved dramatically ($r^2 = 0.91$), and now molecular shape can be accurately fit to empirical toxicity (Figure 2).

The chemical concentrations and the shapes of electronic charge clouds have a fundamental role in the initial chemical reactions responsible for their toxicity and correlation analysis. Interestingly, the best correlation between shape similarity and toxicity was for growth inhibition of the chemicals at 3 mM/l, compared to 12 mM/l and EC_{50} values (Figure 3). Nonetheless, the results show that there is a difference in the correlations with toxicity between the whole molecule and fragment similarities. Higher correlations between fragment similarity and empirical toxicity were observed. Indeed, there are better correlations between fragment similarities than whole molecule similarities for the 12 mM/l and EC_{50} data as well (Figure 3). However, it is important to realize that the whole molecule similarities were for all 13 chemicals, while single fragment similarities had 2 chemicals removed as discussed previously. Indeed, looking at the whole molecule similarity correlation to growth inhibition at 3 mM/l, there are no obvious chemicals that are outliers. By looking at figures 3 and 4 one may realize that there is poor distribution of points for both 3 mM/l and 12 mM/l concentrations, but

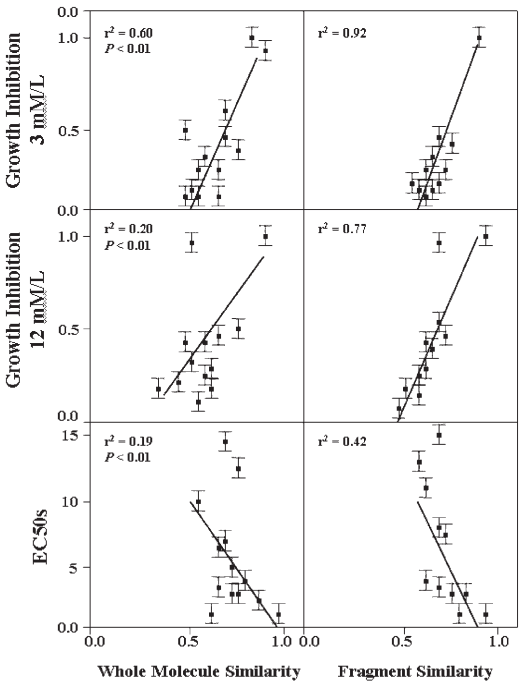

Figure 3. Experimental toxicity vs. whole molecule similarity and fragment similarity with a density range of 10^{-3} to 10^{-1} described for ATQ and h-ATQs.

not for the EC_{50} results. For this reason alone, the EC_{50} results are more preferred.

The results from this part of the correlation analysis showed that data sets for growth inhibition at 3 and 12 mM/l showed good correlations to the shape similarity. However there were poor correlations between the EC_{50} values and the shape data ($r^2 = 0.42$ and 0.19, Figure 3). It is important to note, however, that the slope is negative. As the shape similarities of fragments and/or whole molecules increase, the EC_{50} values decrease (Figure 3). This can be explained by the fact that the chemicals most similar to 2-hATQ also have lower EC_{50} values (higher toxicity and growth inhibition). The higher level of correlation of toxicity with the shape features of the middle ring of these molecules may be due to the fact that ANT and 1,2,10-thANT are not in these correlations. Thus, the low electron density of quinone ring in hATQs and middle ring of ATQ as a potential feature, may explain why toxicity is not being compared to molecules without this feature (e.g. ANT and 1,2,10-thANT).

Among the three correlations of whole molecule similarity and empirical toxicity, the results from 3 mM/l growth inhibition again showed higher regression coefficient than 12 mM/l and EC_{50} values (Figure 3). The r^2 for the regressions suggest that use of growth inhibition 3 mM/l is an important measure of toxicity and is amenable to QSAR analysis. Growth inhibition at 12 mM/l had a weak correlation with whole molecule similarity, however there is one outlier (ANT), presented in the graph which degrades the correlation (Figure 3). The EC_{50} values did not correlate well with whole molecular similarity ($r^2 = 0.19$). In this case one can see that the data falls onto a vertical line where the similarities reach at lower value (Figure 3). In this work, local (fragment) and global shape (whole molecule) could be independently correlated to toxicity. This reflects the fact that the ANT photoproducts do not require photoactivation to be toxic [3]. Viewing figures 3 one may conclude that whole molecule and fragment similarities by themselves in general have weak correlation with experimental toxicities, although the patterns shown indicate the presence of underlying relations for further modelling. To determine if this relation could be better revealed, a hyperbolic fit of the shape data to the toxicity data was performed.

3.3 Hyperbolic fit of molecular shape and toxicity data

The rational to use hyperbolic function was to best fit the molecular shape to the empirical toxicity data. This function spreads out one set of data with respect to another and optimizes the slope between two sets of data. Different analytical functions have been tested, among those, hyperbolic function provide the best fit in our analysis. The hyperbolic function (Eq. 1) was fit to each empirical toxicity data set to solve the constant C_0 and C_1.

$$Y_{theor} = C_0/(1\text{-}C_1X_1) \quad (1)$$

Here X_1 represents either one-ring or whole molecule similarities, and C_0 and C_1 are constants for intercept and slope to fit the shape and toxicity data (Table 3). The optimum values of the coefficients C_0, and C_1 are generated by fitting either the fragment or whole molecule similarities against the experimental toxicities. They were calculated for the whole molecule and the fragment shape similarities based on growth inhibition at 3 and 12 mM/l as well as the EC_{50} values (Table 3). The correlations of Y_{theor} for ANT and the 12 photoproducts vs the empirical toxicity data were quite strong. The correlations in all cases include all 13 chemicals. The six graphs show how the hyperbolic fit of the shape data to toxicity gives excellent correlations (Figure 4). Interestingly, the whole molecule correlations are now as good as those for the fragment similarities (Figures 4). Correlations between whole molecule and fragment similarities with empirical toxicity are highly significant ($p < 0.01$ in all cases). In this inclusive model, with the use of a hyperbolic equation, the adjusted r^2 is high for all six graphical models. This is especially striking for the EC_{50} values, which had essentially no correlation to toxicity (Figure 3).

The results obtained demonstrate that in this QSAR study before use of hyperbolic fit, the correlations of fragment similarities and toxicity data (growth inhibitions at 3, 12 mM/l and EC_{50} values) were better than that for the whole molecules (Figure 3). After use of hyperbolic fit,

Table 3. *The numerical shape analysis and theoretical toxicity (hyperbolic dependencies).* Theoretical toxicity was derived using equation $Y_{theor} = C_0/(1\text{-}C_1X_1)$ from the similarities of (*a*,*b*)-maps shape code of the whole PAH molecules and one-ring fragments to the (*a*,*b*)-maps of the 2-hATQ moleculare and its middle one-ring fragment, respectivley.

Compounds	Hyperbolic Dependencies G.I. (3 mM/L) Whole Molecule Similarity W.M.S (3-1)	Hyperbolic Dependencies G.I. (3 mM/L) Fragment Similarity F.S. (3-1)	Hyperbolic Dependencies G.I. (12 mM/L) W.M.S. (3-1)	Hyperbolic Dependencies G.I. (12 mM/L) F.S. (3-1)	Hyperbolic Dependencies G.I. (EC_{50}s) W.M.S. (3-1)	Hyperbolic Dependencies G.I. (EC_{50}s) F.S. (3-1)
Ant	0.28	0.13	0.6048	0.288	0.504	0.24
ATQ	0.27	0.34	0.6208	0.7857	0.32	0.405
1-hATQ	0.27	0.24	0.405	0.365	1.944	1.752
2-hATQ	0.99	0.99	0.99	0.99	0.05	0.05
1,2-dhATQ	0.14	0.15	0.264	0.284	1.848	1.988
1,3-dhATQ	0.19	0.19	0.333	0.3375	1.85	1.875
1,4-dhATQ	0.05	0.05	0.1452	0.1562	4.29	4.615
1,5-dhATQ	0.03	0.03	0.1056	0.1104	9.9	10.35
1,8-dhATQ	0.15	0.15	0.2911	0.2911	1.775	1.775
2,6-dhATQ	0.01	0.01	0.0552	0.0504	8.28	7.56
1,2,4-thATQ	0.05	0.03	0.1625	0.18	3.9	4.32
1,2,5,8-thATQ	0.06	0.07	0.0969	0.1122	5.415	6.27
1,2,10-thANT	0.03	0.02	0.1725	0.94	6.2	4.7

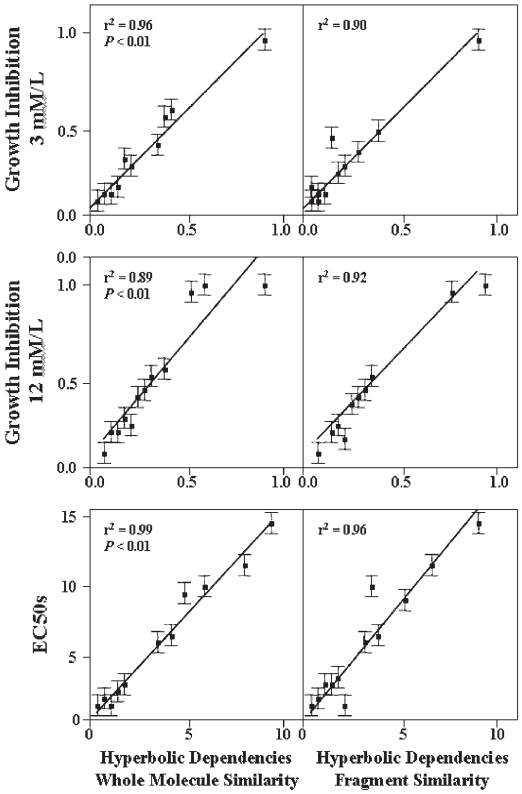

Figure 4. The hyperbolic type dependence shows a strong and almost linear relationship between whole molecule and one ring with experimental toxicity. Hyperbolic dependencies for whole molecule and one-ring similarity described for ANT, ATQ and h-ATQs with density range of 10^{-3} to 10^{-1}.

equally good correlations of the toxicity data to the whole molecule and fragment shape features were observed. The differences between fragment and whole molecule similarities may relate to the ways in which these moieties interact with biological receptors. This may lie in the possible differences in the structures of the chemicals which are consistent with the production of specific biological effects. Both the fragment and whole molecule similarities analyses, without use of hyperbolic fit, resulted in regression models which are reflected in changes in free energy. This is based on the assumption that the structure of a molecule (i.e., its geometric and electronic properties) dictates its ability to interact with organism and ultimately result in inhibition of growth.

The low electronic density in the middle ring is a diagnostic element that may provide a measure of the rapid rate of photooxidation of the molecules. As well this is the most reactive region of the molecules. Thus, since these molecules appear to be toxic without further activation, it is logical that the central ring is an important determinant in toxicity. Conversely, the whole molecule similarity of ANT and its photoproducts may represent their general ability to bind to biological receptors. This is consistent with the ability of these chemicals to bind to specific proteins in the photosynthetic apparatus and inhibit electron transport [3, 25]. Thus, it is logical that both local and global shape features can independently be incorporated into QSARs of toxicity for modified ANT.

3.4 Correlation analysis of photosynthetic activity and molecular shapes

Because both the one ring and whole molecule similarities of ANT, ATQ and the hATQs showed a good correlation with the empirical whole organism toxicity data, it was of interest to compare the molecular shape data to a physiological end point. Further, it was important to determine if

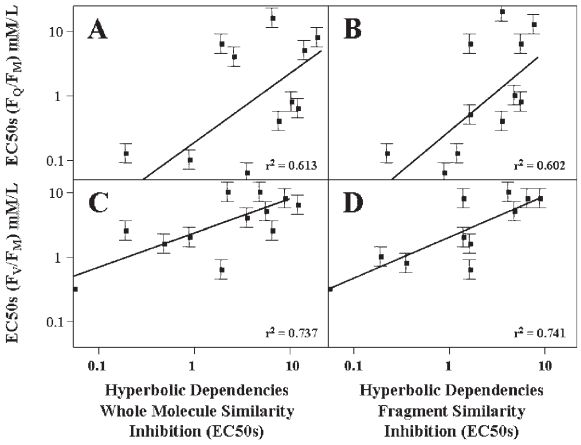

Figure 5. Correlations of (a, b)-maps for one-ring and whole molecule similarities vs F_V/F_M and F_Q/F_M. Hyperbolic fit of the similarities for the EC_{50} values for inhibition of growth were used on the X axis. The relevant photosynthesis data is plotted on the Y axis. A) Correlation of F_Q/F_M with hyperbolic dependencies of whole molecular similarity. B) Correlation analysis of F_Q/F_M with hyperbolic dependencies of one-ring similarity. C) Correlation of F_V/F_M hyperbolic dependencies of vs whole molecular similarity. D) F_V/F_M vs hyperbolic dependencies of one-ring similarity.

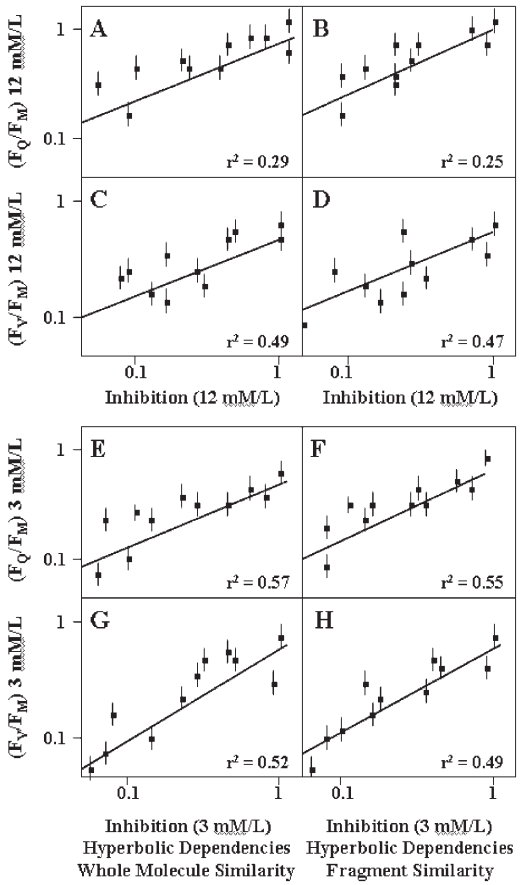

Figure 6. Computed correlation of similarities of (a, b)-maps of one-ring and whole molecule vs F_V/F_M and F_Q/F_M measured at 12 mM/l chemical concentrations, A) Correlation of F_Q/F_M with hyperbolic dependencies of whole molecular similarity. B) Correlation analysis of F_Q/F_M with hyperbolic dependencies of one-ring similarity. C) Correlation of F_V/F_M hyperbolic dependencies of whole molecular similarity. D) F_V/F_M vs hyperbolic dependencies of one-ring similarity. Computed correlation similarities at 3 mM/l chemical concentrations, E) Correlation of F_Q/F_M with hyperbolic dependencies of whole molecular similarity. F) Correlation analysis of F_Q/F_M with hyperbolic dependencies of one-ring similarity. G) Correlation of F_V/F_M hyperbolic dependencies of whole molecular similarity. H) F_V/F_M vs hyperbolic dependencies of one-ring similarity.

the hyperbolic fits for whole organism toxicity would correlate to another endpoint (such as photosynthesis activity) without adjustment of the data. Therefore, the hyperbolic fits of shape data in Table 3 were plotted against data for inhibition of photosynthesis by the chemicals. Inhibition of photosynthetic activity in vivo was assessed previously by use of Chl *a* fluorescence induction [6]. F_V/F_M and F_Q/F_M were used as indicators of photosynthetic activity vs molecular shape similarity. The correlation analysis between molecular shape similarity and photosynthetic activity are shown in figures 5 and 6.

The IC_{50} values for F_V/F_M and F_Q/F_M were plotted against hyperbolic dependencies of one-ring and whole molecule similarity to determine their correlation and predictive capacity. The photosynthetic activity data from a previous study [6] were plotted against hyperbolic dependencies acquired for EC_{50} values from growth inhibition in this study (Table 3). A weak correlation between molecular similarity and inhibition of photosynthetic activity was obtained when the F_Q/F_M was used in the regression (Figure 5 (A–B); $r^2 = 0.613$, 0.602, $p < 0.23$). Hence, this model has some predictive capacity for inhibition of photosynthesis by ANT, ATQ and the hATQs. A better relationship was apparent when F_V/F_M was used (Figure 5 (C–D); $r^2 = 0.737$, 0.741). This indicates that theoretical basis exists for the dependence of photosynthetic activity and molecular similarity.

F_V/F_M was found to be a better indicator of acute toxicity than F_Q/F_M. Nonetheless, it is important that the two data sets for F_Q/F_M and F_V/F_M have reasonable regression coefficients (Figure 5), as both F_Q/F_M and F_V/F_M were found to be excellent bioindicators of effects. The results with the chemicals at 12 mM/l revealed again that F_V/F_M had higher correlations to the shape data than F_Q/F_M (Figure 6; A, B, C, D), even though F_Q/F_M is a more sensitive indicator of photosynthetic activity. The correlation of F_Q/F_M with hyperbolic dependencies for whole molecule and fragment similarity at 12 mM/l is not statistically significant and provides a low level of regression coefficient ($r^2 = 0.29$ and 0.25).

The correlation analysis of photosynthetic activities at 3 mM/l and chemical shape had reasonably strong correlations (Figure 6; E, F, G, H). Interestingly, the FQ/FM correlations are now slightly better than those for FV/FM.

This is consistent with F_Q/F_M value that brings a better measure of chronic toxicity [6]. Thus, at lower concentration we would expect to have a better fit to the shape data.

The results of previous studies [15, 16, 22, 26] and the work related here show that molecular similarities of hATQs correlate with indicators of photosynthetic activity (F_V/F_M and F_Q/F_M) (Figures 5 and 6). Interestingly, both the global and local shape features correlated equally well with the photosynthesis data. This is again consistent with direct action of these chemicals on the photosynthetic apparatus [6]. Importantly, this part of the research showed that a QSAR model based on whole organism toxicity correlated well with inhibition at the putative site of action of these chemicals. This tends further credence to the supposition that the primary site of action of these compounds is the photosynthetic apparatus.

4 Conclusions

Polycyclic aromatic hydrocarbons (PAHs) are common environmental pollutants that are of concern because they are suspected toxicants and carcinogens. Our attempt was to explore the potential of developing a PAH photoinduced toxicity QSAR by examination of our existing toxicity data and their correlation with molecular descriptors. This was followed by development of a high quality self-consistent database of molecular shapes and kinetic parameters for anthracene and oxygenated anthracenes in aqueous systems and use of these data to develop and validate a QSAR model. The QSAR approach is being applied to toxicity data and bioenergetics pathways because the electron density stores all the information about each molecule. A detailed electron density shape analysis has been carried out using Shape Group methods [15, 16]. Electron density shape maps obtained by molecular shape analysis can be compared to PAH (ANT, dhATQ) data sets to explain a particular physical, chemical, toxicological or carcinogenic property.

Acknowledgements

This study has been supported by the Canadian Network of Toxicology Centers and by a research grant from the Natural Sciences and Engineering Research Council of Canada. The fourth author acknowledges financial support from a Sterge Faculty Fellowship.

References

[1] J. M. Neff, *Polycyclic aromatic hydrocarbons in the aquatic environment: Sources, fates, and biological effect,* Applied Science Publishers, London, **1979**.
[2] B. J. Eadie, Distribution of PAHs in Great Lakes, in: J. O. Nriagu (Ed.), *Advances in Environmental Science and Technology*, John Wiley and Sons, **1984**, *14*, 195 – 211.
[3] A. Mallakin, B. J. McConkey, G. Miao, B. Mckibben, V. Snieckus, D. G. Dixon, B. M. Greenberg, *Ecotox. Environ. Safe.* **1999**, *43***,** 204 – 212.
[4] X.-D. Huang, B. J. McConkey, S. T. Babu, B. M. Greenberg, *Environ. Toxicol. Chem.* **1997a**, *8*, 1707 – 1715.
[5] A. Mallakin, D. G. Dixon, B. M. Greenberg, *Chemosphere* **2000**, *40*, 131 – 137.
[6] A. Mallakin, S. T. Babu, D. G. Dixon, B. M. Greenberg, *Environ. Toxicol.* **2002**, *17*, 462 – 471.
[7] P. Hohenberg, W. Kohn, *Phys. Rev.* **1964**, *136*, B864-B871.
[8] P. G. Mezey, *Mol. Phys.* **1999**, *96*, 169 – 178.
[9] P. M. Dean, *Molecular foundation of drug-receptor interaction*, University Press, Cambridge, **1987**.
[10] P. G. Mezey, *J. Mol. Struct. (Theochem)* **1986**, *138*, 13 – 21.
[11] P. G. Mezey, *J. Comput. Chem.* **1987**, *8*, 462 – 469.
[12] P. G. Mezey, *Methods of molecular shape similarity and topological shape design*, in: P. M. Dean (Ed.), *Molecular Similarity in Drug Design*, Chapman & Hall-Blackie Publishers, Glasgow, **1995**, pp. 241 – 268.
[13] P. D. Walker, P. G. Mezey, *J. Comput. Chem.* **1995**, *16*, 1238 – 1249.
[14] M. A. Johnson, G. M. Maggiora (Eds.), *Concepts and Applications of Molecular Similarity*, Wiley Inter-Science, New York, **1990**.
[15] P. G. Mezey, Z. Zimpel, P. Warburton, P. D. Walker, D. Irvine, D. G. Dixon, B. M. Greenberg, *J. Chem. Inf. Comput. Sci.* **1996**, *36*, 602 – 611.
[16] P. G. Mezey, Z. Zimpel, P. Warburton, P. D. Walker, D. G. Irvine, X-D Huang, D. G. Dixon, B. M. Greenberg, *Environ. Toxicol. Chem.* **1998**, 17, 1207 – 1215.
[17] R. G. Pearson, *Acc. Chem. Res.* **1993**, *26*, 250 – 256.
[18] R. G. Par, Z. Zhou. *Acc. Chem. Res.* **1993**, *26*, 256 – 258.
[19] O. G. Mekenyan, G. T. Ankley, G. D. Veith, D. J. Call, *SAR QSAR Environ. Res.* **1994**, *2*, 237 – 247.
[20] O. G. Mekenyan, G. T. Ankley, G. D. Veith, D. J. Call, *SAR QSAR Environ. Res.* **1995**, *4,* 139 – 145.
[21] P. G. Mezey, Dynamic shape analysis of biomolecules using topological shape codes, in: J. Bertan (Ed.), *The role of computational models and theories in biotechnology*, Kluwer Academic Publishers, Dordrecht, **1992**, pp. 83 – 104.
[22] P. G. Mezey, *Shape in Chemistry; An Introduction To Molecular Shape and Topology*, VCH, Weinheim, **1993**.
[23] P. G. Mezey, P. D. Walker, *Drug Discov. Today* **1997**, *2*, 6 – 11.
[24] R. Carbo, (Ed.), *Molecular similarity and reactivity: from quantum chemical to phenomenological approaches*, Kluwer Academic Publishers, Netherlands, **1995**.
[25] P. D. Walker, G. A. Arteca, P. G. Mezey, *J. Comput. Chem.* **1991**, *12*, 220 – 230.
[26] S. N. Krylov, X-D Haung, L. F. Zeiler, D. G. Dixon, B. M. Greenberg, *Environ. Toxicol. Chem.* **1997**, *16*, 2283 – 2295.

